Control of structure formation in phase-separating systems

Awaneesh Singh, A. Mukherjee, H. M. Vermeulen, G. T. Barkema, and Sanjay Puri

Related Articles

Oxygen vacancy segregation and space-charge effects in grain boundaries of dry and hydrated BaZrO3
Appl. Phys. Lett. 100, 061903 (2012)

Phase separation dynamics in a two-dimensional magnetic mixture
J. Chem. Phys. 136, 024502 (2012)

Pressure-energy correlations in liquids. V. Isomorphs in generalized Lennard-Jones systems
J. Chem. Phys. 134, 164505 (2011)

Modeling phosphorus diffusion gettering of iron in single crystal silicon
J. Appl. Phys. 105, 023510 (2009)

Use of an enhanced bulk diffusion-based algorithm for phase separation of a ternary mixture
J. Chem. Phys. 129, 184115 (2008)

Additional information on J. Chem. Phys.

Journal Homepage: http://jcp.aip.org/

Journal Information: http://jcp.aip.org/about/about_the_journal

Top downloads: http://jcp.aip.org/features/most_downloaded

Information for Authors: http://jcp.aip.org/authors

Control of structure formation in phase-separating systems

Awaneesh Singh,[1] A. Mukherjee,[1] H. M. Vermeulen,[2] G. T. Barkema,[2,3] and Sanjay Puri[1,a)]

[1]*School of Physical Sciences, Jawaharlal Nehru University, New Delhi 110067, India*
[2]*Institute for Theoretical Physics, Utrecht University, Leuvenlaan 4, 3584 CE Utrecht, The Netherlands*
[3]*Instituut-Lorentz, Leiden University, Niels Bohrweg 2, 2333 CA Leiden, The Netherlands*

In this paper, we study the evolution of phase-separating binary mixtures which are subjected to alternate cooling and heating cycles. An initially homogeneous mixture is rapidly quenched to a temperature $T_1 < T_c$, where T_c is the critical temperature. The mixture undergoes phase separation for a while and is then suddenly heated to a temperature $T_2 > T_c$. These cycles are repeated to create a domain morphology with multiple length scales, i.e., the structure factor is characterized by multiple peaks. For phase separation in $d = 2$ systems, we present numerical and analytical results for the emergence and growth of this multiple-scale morphology. © *2011 American Institute of Physics.* [doi:10.1063/1.3530784]

I. INTRODUCTION

Consider a binary (AB) mixture, which is homogeneous (or disordered) at high temperatures and phase-separated (or ordered) at low temperatures. If the homogeneous mixture is rapidly quenched below the critical temperature T_c, it becomes thermodynamically unstable. Then, the mixture undergoes phase separation via the formation and growth of domains of A- and B-rich phases. Much research interest has focused on this far-from-equilibrium evolution.[1,2] There now exists a good understanding of segregation dynamics for binary mixtures.[3–7] In cases where phase separation is driven by diffusion, these coarsening processes may be modeled using kinetic Ising models with locally conserved magnetization, e.g., the spin-exchange Kawasaki–Ising model.[2,8,9] The possible spin values ($s = \pm 1$) represent the two species of particles that are demixing. The coarse-grained order parameter (magnetization) of such models is described by the *Cahn–Hilliard–Cook* (CHC) equation[10,11] or *Model B*.[12] In the dilute limit, where droplets of the minority phase grow in a homogeneous background, Lifshitz and Slyozov (LS) have shown that the average domain size increases as $L(t) \sim t^{\phi}$, where t is the time after the quench and $\phi = 1/3$.[13] Huse[14] has shown that the LS growth law also applies to the case where there are approximately equal fractions of the two phases.

Apart from the domain growth laws, experimentalists are also interested in quantitative features of the phase-separating morphologies. An important experimental quantity is the time-dependent structure factor $S(\vec{k}, t)$ ($\vec{k}$ being the wave vector) or its Fourier transform, the correlation function $C(\vec{r}, t)$. Our understanding of $S(\vec{k}, t)$ for a phase-separating system is relatively limited. The structure factor exhibits dynamical scaling, $S(\vec{k}, t) \simeq L^d f(kL)$, where d is the dimensionality. It has a single peak at the inverse of the characteristic length scale, $k_m \sim L(t)^{-1}$. With the passage of time, $k_m \rightarrow 0$ as $k_m \sim t^{-\phi}$. We also know the behavior of $S(\vec{k}, t)$ in the limits $k \rightarrow 0$ [i.e., $S(\vec{k}, t) \sim k^4$] (Refs. 15 and 16) and $k \rightarrow \infty$ [i.e., $S(\vec{k}, t) \sim k^{-(d+1)}$]. The latter result is known as Porod's law and is a result of scattering from sharp interfaces.[17] However, there is still no theory which describes the complete functional form of $S(\vec{k}, t)$.

In this paper, we study the phase-separation dynamics of a binary mixture with a specific interest in the structure factor. In particular, we study the effect of a time-dependent variation of temperature on $S(\vec{k}, t)$. There have been several studies of phase separation with a time-dependent temperature.[18–20] The general question which motivates our study is whether it is possible to create a domain morphology with a predefined structure factor by temporal variation of external parameters. This issue is of great technological importance, especially in the context of tailoring microstructures and nanostructures. For instance, the microstructure of food, paint, or biomaterials is not solely a function of the constituents. It is often an arrested morphology, which is determined by external conditions which guide the structural evolution. Thus, the variation of these external conditions during the structure formation can steer the microstructure in desirable directions, e.g., more durable biomaterials, low-calorie food with better "mouthfeel" and "chewability," and paint with a color that is less sensitive to the method of application (painting or spraying). The present study is a first step in the direction of structure control by temporal variation of external parameters.

In this context, we study phase separation via computer simulations of (a) the conserved Kawasaki–Ising model and (b) the CHC model. In contrast to most earlier studies of this problem, we change external parameters (e.g., temperature) during the simulation to influence the shape of the structure factor. We consider a simple protocol for variation of the temperature, viz., the temperature is cycled between high and low values. Depending on the frequency and amplitude of the cycling, we obtain structure factors with multiple peaks, instead of the usual single peak.

This paper is organized as follows. In Sec. II, we present comprehensive Monte Carlo (MC) results for the Kawasaki–Ising model subjected to a cyclical variation of the temperature. We also present analytical arguments to understand the evolution of the structure factor and correlation function during the heating part of the cycle. In Sec. III, we present analogous results for the CHC model, which is the coarse-grained counterpart of the Kawasaki–Ising model. Finally, Sec. IV concludes this paper with a summary and discussion.

II. PHASE SEPARATION IN THE KAWASAKI–ISING MODEL WITH A TIME-DEPENDENT TEMPERATURE

A binary (AB) mixture is usually described by the Ising model, with Hamiltonian

$$H = -J \sum_{\langle ij \rangle} s_i s_j, \qquad s_i = \pm 1. \tag{1}$$

Here, s_i denotes the spin variable at site i. We consider two-state spins: $s_i = +1$ denotes an A-atom and $s_i = -1$ denotes a B-atom. If the exchange interaction J is positive, the system segregates into A- and B-rich regions below the miscibility gap. In Eq. (1), the subscript $\langle ij \rangle$ denotes a summation over nearest-neighbor pairs i and j. The total magnetization $M = \sum_{i=1}^{N} s_i$ ($= N_A - N_B$, where N_A and N_B are total numbers of A and B, respectively) is a conserved quantity. We associate stochastic dynamics with the Ising model by placing it in contact with a heat bath. The appropriate dynamics for the phase-separation problem is spin-exchange kinetics or Kawasaki kinetics.[8,9]

It is straightforward to implement an MC simulation of the Ising model with spin-exchange kinetics. In a single step of MC dynamics, we choose at random a pair of adjacent spins on the lattice. The change in energy δH that would occur if the spins were exchanged is computed. The step is then accepted or rejected with the Metropolis acceptance probability[21,22]

$$P = \begin{cases} e^{-\beta \delta H}, & \text{if } \delta H \geq 0, \\ 1, & \text{if } \delta H < 0. \end{cases} \tag{2}$$

Here, $\beta = (k_B T)^{-1}$ denotes the inverse temperature. In the simulations reported here, the temperature has a time-dependent form $T(t)$. This stochastic move is repeated many times. One Monte Carlo step (MCS) is completed when this algorithm is performed N times (where N is the total number of spins), regardless of whether the move is accepted or rejected.

All our simulations have been performed on a two-dimensional (2D) Kawasaki–Ising model, defined on a square lattice of size L^2 ($L = 512$) with periodic boundary conditions. The statistical quantities presented here (e.g., correlation function and structure factor) are obtained as averages over ten independent runs on systems of size 512^2. Each run starts with a randomly mixed state with equal numbers of up and down spins ($\rho = 0.5$ is the density of up or down spins, which corresponds to a mean magnetization $m = 0$). At time $t = 0$, the system is quenched to a temperature $T = 1.5$, measured in units of J ($T_c \simeq 2.269$ for the 2D Ising model on

a square lattice). After the system has evolved for time t_1, we heat the system to $T = \infty$ (first heating) and allow it to evolve until time t_2. Therefore, the duration of the first heating period is $t_2 - t_1$. The system is then quenched again to $T = 1.5$ (second quench until time t_3) and then heated again (second heating until time t_4), etc. The precise temperature protocol followed in different simulations will be specified at the appropriate place. We should mention that the instantaneous quenches and heating considered here are idealizations of the experimental situation. In practice, temperature changes occur on nonzero time-scales, which can have interesting physical consequences.[23]

A. First quench

In Fig. 1(a), we show the evolution of the system after a quench to $T = 1.5$ at $t = 0$. The snapshot corresponds to $t = 10^6$ MCS. Regions with $s_i = +1$ (A-rich) and $s_i = -1$ (B-rich) are marked in black and white, respectively. The structure of the evolving system is characterized by the correlation function

$$C(\vec{r}_i, \vec{r}_j; t) \equiv \langle s_i s_j \rangle - \langle s_i \rangle \langle s_j \rangle = \langle s_i s_j \rangle - m^2. \tag{3}$$

Here, the angular brackets denote an averaging over the initial ensemble and different noise realizations. As the system is translationally invariant, the correlation function depends only on $\vec{r} = \vec{r}_j - \vec{r}_i$,

$$C(\vec{r}_i, \vec{r}_j; t) = C(\vec{r}_i, \vec{r}_i + \vec{r}; t) = C(\vec{r}, t). \tag{4}$$

Actually, most experiments study the structure factor, which is the Fourier transform of the correlation function,

$$S(\vec{k}, t) = \sum_{\vec{r}} e^{i \vec{k} \cdot \vec{r}} C(\vec{r}, t). \tag{5}$$

Since the system is isotropic, we can improve statistics by spherically averaging the correlation function and the structure factor. The corresponding quantities are denoted as $C(r, t)$ and $S(k, t)$, respectively. In Figs. 1(b) and 1(c), we show the correlation function [$C(r, t)$ vs r] and the structure factor [$S(k, t)$ vs k] for three different times. Notice that we do not present here the usual scaling plot, where datasets at different times collapse onto a master function.[24,25] The structure factor in Fig. 1(c) contains information about the presence of sharp interfaces (defects) in the phase ordering system. The tail of the structure factor decays as $S(k, t) \sim k^{-3}$, which is Porod's law in $d = 2$. The Porod tail only persists up to values of k corresponding to the typical width of the wall, $k < \xi^{-1}$. Figure 1 will serve as a reference point for later results, obtained for a variety of cooling–heating cycles.

Finally, let us examine the time-dependence of the characteristic domain size $L(t)$. There are many equivalent definitions for measuring the domain size. For example, $L(t)$ can be defined as the point where the correlation function in Fig. 1(b) first crosses zero. Alternatively, we can define the length scale as the inverse of the location of the structure-factor peak [$L(t) \sim k_m^{-1}$] or the inverse of the first moment of the structure factor [$L(t) \sim \langle k \rangle^{-1}$]. All these definitions are equivalent in the scaling regime. In this paper, we use the definition $L \sim k_m^{-1}$. In Fig. 1(d), we show the time-dependence
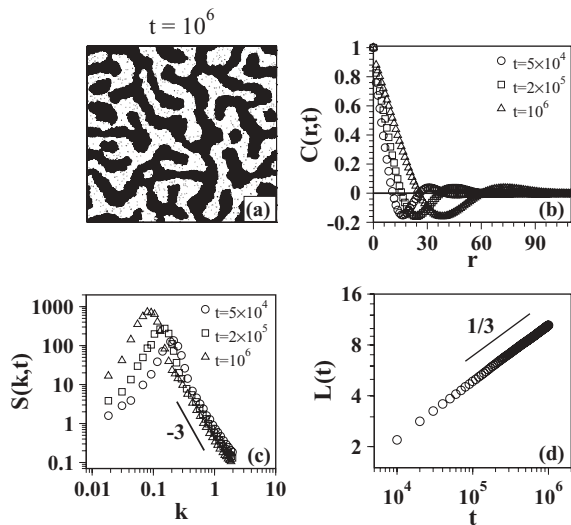
FIG. 1. (a) Evolution snapshot from a simulation of the Kawasaki–Ising model. The details of the simulation are provided in the text. The system size is 512^2 and periodic boundary conditions are applied in both directions. The system was quenched from $T = \infty$ to $T = 1.5$ at time $t = 0$. The up spins (A-atoms) are marked in black, whereas the down spins (B-atoms) are unmarked. (b) Correlation function data [$C(r, t)$ vs r] at three different times after the first quench. (c) Structure-factor data [$S(k, t)$ vs k] for the same times as in (b). The line of slope -3 denotes the Porod tail in $d = 2$, $S(k, t) \sim k^{-3}$ as $k \to \infty$. The Porod tail applies for scattering of sharp interfaces, i.e., for k-values which satisfy $\xi^{-1} \gg k \gg L^{-1}$, where ξ is the interfacial thickness. In our simulations, $\xi \sim O(1)$. (d) Time-dependence of domain size [$L(t)$ vs t] for the evolution depicted in (a). The line of slope $1/3$ denotes the LS growth law, $L(t) \sim t^{1/3}$.

of the length scale on a log–log plot. We see that the domain growth depicted in Fig. 1(a) is consistent with the LS growth law, $L(t) \sim t^{1/3}$. Thus, at the end of the first heating, $L(t_1) \simeq (\gamma t_1)^{1/3}$, where γ is the surface tension at the AB interface.

B. First heating

After the system shown in Fig. 1(a) has evolved for time $t_1 = 10^6$ MCS, we suddenly heat the system to $T = \infty$ ($\beta = 0$). The preferred equilibrium structure is now in the homogeneous state, and the domain structure will start melting. At $T = \infty$, all proposed spin exchanges will be accepted. On the average, each spin pair is exchanged once during one MCS. This means that every particle will make two steps, either along the x- or y-axis. Therefore, within a few MCS, the domain walls get fuzzier and domains become less distinctive. Inside a domain, the concentration of particles with opposite spin increases.

We start the first heating with the final configuration (at $t_1 = 10^6$ MCS) in Fig. 1(a). We evolve the system for 700 MCS at temperature $T = \infty$. The snapshots of the resultant disordering dynamics are shown in Fig. 2. In Fig. 3(a), we show the evolution of the structure factor during the heating process in Fig. 2. We see that the structure factor retains a peak at small values of k after heating for 700 MCS. The peak amplitude becomes lower as heating proceeds, and its position shifts to smaller values of k, i.e., the length scale increases. We will explain this behavior shortly. The large
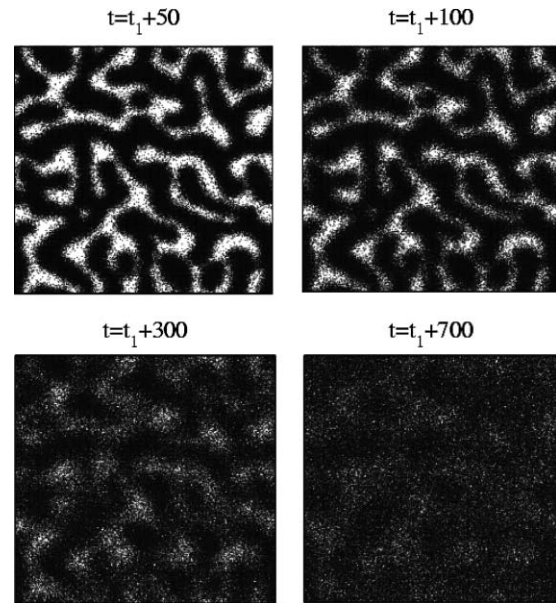
FIG. 2. Evolution snapshots from the Kawasaki–Ising model during the first heating period. The system was heated to $T = \infty$ at time $t_1 = 10^6$ MCS, corresponding to the snapshot in Fig. 1(a). From top left, the frames show the system at $t = t_1 + 50$, $t_1 + 100$, $t_1 + 300$, and $t_1 + 700$ MCS.

values of k correspond to small-scale structure, which is seen to become disordered as the corresponding $S(k, t)$ is flat. A homogeneous system of spins with magnetization $m = 0$ (i.e., the initial state for the first quench) has $S(\vec{k}, 0) = 1$ in our units—the corresponding dataset is denoted by a dashed line in Fig. 3(a). The corresponding correlation function is $C(\vec{r}, 0) = \delta_{\vec{r}, 0}$. The solid lines superposed on the datasets for $t = t_1 + 100$, $t_1 + 300$, and $t_1 + 700$ (during heating) will be explained shortly. The time-dependence of the length scale during the first heating is shown in Fig. 3(b).

We would like to know how the heating process influences the structure factor of the system. In other words, if $S(\vec{k}, t_1)$ is the structure factor when heating starts, is it possible to predict $S(\vec{k}, t)$ for $t > t_1$? Recall that the particles are performing random walks in $d = 2$. After t MCS of heating, the average displacement of a particle is $\sqrt{2t}$. The corresponding probability distribution for a particle to be displaced
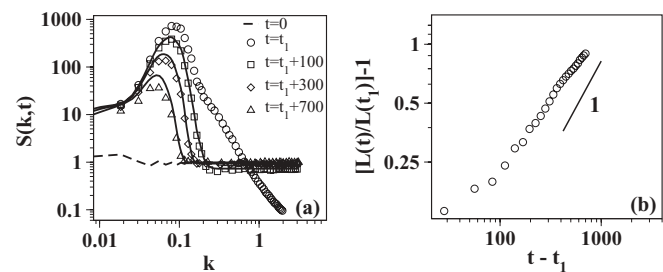

FIG. 3. (a) Structure-factor data for three different times during the first heating period shown in Fig. 2: $t = t_1 + 100$, $t_1 + 300$, and $t_1 + 700$ MCS. The solid lines superposed on these datasets denote the expression in Eq. (11), with $S(k, t_1)$ obtained numerically. For comparison, we also plot the structure factor of the initial disordered state ($t = 0$) and the structure factor at the end of the first quench, $t_1 = 10^6$ MCS. (b) Time-dependence of domain size [$L(t)/L(t_1) - 1$ vs $t - t_1$] during the first heating period at temperature $T = \infty$. The duration of the first heating period is 700 MCS.

(x, y) from its initial position is

$$g_{\tilde{\sigma}}(x, y) = g_{\tilde{\sigma}}(x) g_{\tilde{\sigma}}(y)$$

$$= \frac{1}{\sqrt{2\pi\tilde{\sigma}^2}} e^{-x^2/(2\tilde{\sigma}^2)} \cdot \frac{1}{\sqrt{2\pi\tilde{\sigma}^2}} e^{-y^2/(2\tilde{\sigma}^2)}, \quad (6)$$

where $\tilde{\sigma} = \sqrt{2t}$. The correlation function changes over time by convolution with the Gaussian distribution. The predicted correlation function after $(t - t_1)$ MCS of heating is

$$C(x, y, t) = C(x, y, t_1) * g_\sigma(x) * g_\sigma(y)$$

$$= \frac{1}{2\pi\sigma^2} \int_{-\infty}^{\infty} dx' \int_{-\infty}^{\infty} dy' C(x', y', t_1)$$

$$\times \exp\left[-\frac{(x - x')^2 + (y - y')^2}{2\sigma^2}\right], \quad (7)$$

where $\sigma^2 = 2(t - t_1)$. The above expression only applies for $r = \sqrt{x^2 + y^2} > 0$. In polar coordinates,

$$C(r, t) = \frac{e^{-r^2/(2\sigma^2)}}{2\pi\sigma^2} \int_0^{\infty} dr' r' C(r', t_1) e^{-r'^2/(2\sigma^2)}$$

$$\times \int_0^{2\pi} d\theta' \exp\left(\frac{rr' \cos\theta'}{\sigma^2}\right)$$

$$= \frac{e^{-r^2/(2\sigma^2)}}{\sigma^2} \int_0^{\infty} dr' r' C(r', t_1) e^{-r'^2/(2\sigma^2)}$$

$$\times I_0\left(\frac{rr'}{\sigma^2}\right), r > 0, \quad (8)$$

where $I_0(z)$ is the zeroth-order modified Bessel function.[26]

For $r = 0$, we always have $C(r = 0, t) = 1$. This is clear from the definition in Eq. (3) as $s_i^2 = 1$ and $m = 0$ for a critical quench. In Fig. 4(a), we show simulation data for the correlation function at three different times in the first heating period. The solid lines denote the expression in Eq. (8), where $C(r, t_1)$ is obtained numerically. There is an excellent agreement between the simulation data and Eq. (8).

Next, we consider the structure factor, which is the Fourier transform of the correlation function. On the discrete lattice, we have for the correlation function [analogous to Eq. (7)]
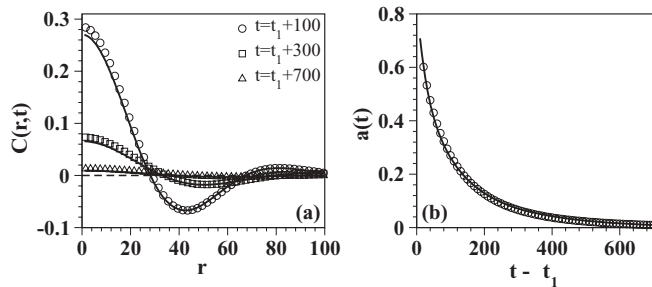
$$C(\vec{r}, t) = \sum_{\vec{r}'} C(\vec{r}', t_1) \exp\left[-\frac{(\vec{r} - \vec{r}')^2}{2\sigma^2}\right]$$

$$+ [1 - a(t)]\delta_{\vec{r},0}, \quad (9)$$

where we have explicitly included the case $\vec{r} = 0$. Here,

$$a(t) = \sum_{\vec{r}'} C(\vec{r}', t_1) \exp\left(-\frac{\vec{r}'^2}{2\sigma^2}\right). \quad (10)$$

The decay of $a(t)$ with t is shown in Fig. 4(b). The corresponding expression for $S(\vec{k}, t)$ is

$$S(\vec{k}, t) = \sum_{\vec{r}} e^{i\vec{k}\cdot\vec{r}} \sum_{\vec{r}'} C(\vec{r}', t_1) \exp\left[-\frac{(\vec{r} - \vec{r}')^2}{2\sigma^2}\right]$$

$$+ 1 - a(t) \simeq S(\vec{k}, t_1)e^{-k^2\sigma^2/2} + 1 - a(t). \quad (11)$$

In Fig. 3(a), we have shown $S(k, t)$ vs k for three times in the first heating period. The solid lines in Fig. 3(a) denote the expression in Eq. (11), with $S(k, t_1)$ obtained numerically. They are seen to be in excellent agreement with the numerical data. Notice that the Porod tail immediately disappears as we start heating. This is because the interfaces become fuzzy as particles at the interfaces start performing random walks. The flat portion of the structure factor has the value $S(k, t) \simeq 1 - a(t)$, which corresponds to the difference between $C(\vec{r} = 0, t) = 1$ and $\lim_{r \to 0} C(r, t) = a(t)$ in Fig. 4(b). As $t \to \infty$, $a(t) \to 0$ and $S(k, t) \simeq 1$, which corresponds to the initial homogeneous state in Fig. 3(a).

Recall that the inverse of the structure-factor peak measures the length scale, which is shown in Fig. 3(b). To understand how the length scale changes with time during the heating period, we estimate the peak location [denoted as $k_m(t)$] from the expression for $S(\vec{k}, t)$ in Eq. (11),

$$\frac{d}{dk}S(k, t)\bigg|_{k=k_m} \simeq \frac{d}{dk}S(k, t_1)\bigg|_{k=k_m} e^{-k_m^2\sigma^2/2}$$

$$+ S(k_m, t_1)e^{-k_m^2\sigma^2/2}(-k_m\sigma^2) = 0. \quad (12)$$

We can expand $S(k, t_1)$ about its peak position $k_0 = k_m(t_1)$ as

$$S(k, t_1) \simeq S(k_0, t_1) + \frac{(k - k_0)^2}{2} S''(k_0, t_1) + O[(k - k_0)^4], \quad (13)$$

where $S''(k_0, t_1) < 0$. Replacing Eq. (13) in Eq. (12), we obtain

$$k_m(t) \simeq \frac{k_0 S''(k_0, t_1)}{S''(k_0, t_1) - \sigma^2 S(k_0, t_1)}$$

$$= \frac{k_0}{1 + 2(t - t_1)S(k_0, t_1)/S''(k_0, t_1)}. \quad (14)$$

FIG. 4. (a) Correlation function data $[C(r, t)$ vs $r]$ at three different times during the first heating period shown in Fig. 2. The solid lines denote the functional form in Eq. (8) with $C(r, t_1)$ (correlation function at the end of the first quench) obtained numerically. (b) Decay of $a(t)$ with $t - t_1$ during the first heating. The solid line denotes $C(0, t)$ from Eq. (8). The asymptotic behavior is described by $a(t) \sim (t - t_1)^{-2}$.

Equation (14) shows how the length scale increases with time during the heating period,

$$L(t) \simeq L(t_1) \left[1 + 2(t - t_1) \frac{S(k_0, t_1)}{S''(k_0, t_1)} \right]. \quad (15)$$

Our data in Fig. 3(b) are consistent with this growth law. Notice that as the peak becomes softer with time, we will have to include higher terms of the Taylor expansion in Eq. (13) at later times.

The peak strength also diminishes as the structure melts during heating. The melting time t_m can be estimated as the period in which a random walker traverses the domain scale $L(t_1)$, i.e.,

$$t_m \simeq L(t_1)^2. \quad (16)$$

Therefore, if we desire to retain any structure at the end of the heating period, we must have $t_2 - t_1 < t_m$. The above arguments can easily be generalized to the cases of second quench, second heating, etc. The duration of the first quench sets the possible time-windows for subsequent operations.

C. Second quench

In a single-quench experiment, the small-distance structure corresponds to the large-k part of the structure factor. This is the region where domain formation begins, with a peak emerging at large k and moving to smaller values of k as time progresses. As we have seen earlier, the large-k region after heating [see Fig. 3(a)] resembles the homogeneous initial condition of a single-quench experiment. The heating process breaks up the domain structure, starting from the smallest length scales, and progressing to larger length scales. We expect that we can grow a second peak by continuing the evolution of the heated system in Sec. II B at a lower temperature. Therefore, we undertake a second quench at time t_2. Again, the system is cooled to the temperature $T = 1.5$.

Recall that we started our simulation with a homogeneous system having $m = 0$. This system was evolved at $T = 1.5$ for $t_1 = 10^6$ MCS. Subsequently, it was heated for 700 MCS ($t_2 = t_1 + 700$) at $T = \infty$. Now, the temperature has been quenched again to $T = 1.5$. The evolution snapshots for this second quench are shown in Fig. 5. The snapshots at $t = t_2 + 200$ MCS and $t = t_2 + 2000$ MCS clearly show the existence of structure on two length scales. As we will see shortly, this two-scale morphology is characterized by a structure factor with two peaks.

The structure factor of a homogeneous system with equal number of up and down spins ($m = 0$) is $S(\vec{k}, 0) \simeq 1$. It is clear from Fig. 3(a) that it requires some amount of heating before the large-k part of $S(\vec{k}, t)$ reaches the value 1. We perform the second quench before $S(\vec{k}, t) \to 1$ due to heating. The evolution of the corresponding two-peak structure factor is shown in Fig. 6(a). Notice that one of the peaks at k_1 (corresponding to the large-scale structure) is almost static, whereas the other peak at k_2 (corresponding to the small-scale structure) moves with time. The time-dependence of the relevant length scales, defined as $L_1 = k_1^{-1}$ and $L_2 = k_2^{-1}$, is shown in Fig. 6(b).
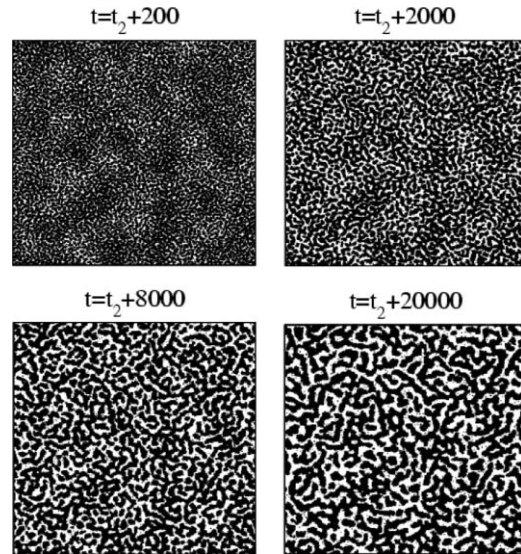

FIG. 5. Evolution snapshots during the second quench period. The quench occurs at $t_2 = t_1 + 700$ MCS—the initial state is shown in the last snapshot of Fig. 2. The snapshots shown here correspond to $t = t_2 + 200$, $t_2 + 2000$, $t_2 + 8000$, and $t_2 + 20\,000$ MCS.

The flat region of the structure factor during first heating, $S(\vec{k}, t) < 1$, characterizes a homogeneous system with mean magnetization different from 0. Recall from Eq. (11) that the flat portion of the structure factor is

$$S(\vec{k}, t) \simeq 1 - a(t), \quad (17)$$

where $a(t) \to 0$ as the heating continues. Therefore, the effective magnetization of the corresponding homogeneous system is

$$m_{\text{eff}}(t) = \sqrt{a(t)}, \quad (18)$$

and the effective density is

$$\rho_{\text{eff}} = \frac{1 + \sqrt{a(t)}}{2}. \quad (19)$$

We can now obtain a better understanding of the growth of the second peak during the second quench. The heating period during first heating was 700 MCS. At the end of this time period, we estimate the flat portion of the structure factor as $S(\vec{k}, t) \simeq 0.98$ from Fig. 3(a). This corresponds to
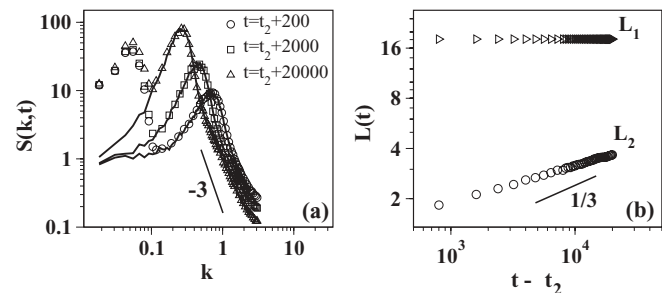

FIG. 6. (a) Structure factors at $t = t_2 + 200$, $t = t_2 + 2000$, and $t_2 + 20\,000$ MCS during the second quench period (see Fig. 5). The solid lines denote the structure factors obtained from a single-quench simulation at $t = 2000$, 20 000 MCS. The initial condition for this simulation was slightly off-critical with $m_{\text{eff}} \simeq 0.14$. (b) Time-dependence of domain sizes during the second quench period.
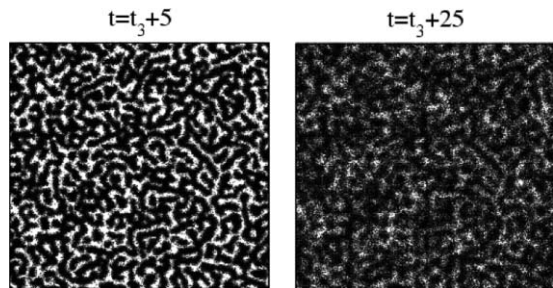
FIG. 7. Evolution snapshots during the second heating period, which starts at $t_3 = t_2 + 20\,000$ MCS—the initial state is shown in the final snapshot of Fig. 5.

FIG. 9. Evolution snapshots during the third quench period. The quench occurs at $t_4 = t_3 + 25$ MCS—the initial state is shown in the final snapshot of Fig. 7.

$m_{\mathrm{eff}} \simeq 0.14$. For purposes of comparison, we undertake a conventional first-quench simulation of phase separation at $T = 1.5$. The initial condition consists of a homogeneous off-critical mixture with $m_{\mathrm{eff}} \simeq 0.14$. In Fig. 6(a), we compare the two-peak structure factor from our second-quench simulation with the usual one-peak structure factor from the off-critical ($m_{\mathrm{eff}} \simeq 0.14$) simulation. Other than the first peak, the structure factors are in excellent agreement.

The above results clarify the general scenario. The first quench leads to conventional phase-separation dynamics. When the system is heated, the domains homogenize (melt at small length scales), but an imprint of the larger domain scale survives. The second quench leads to the re-emergence of domains from the homogeneous or disordered state. This growth process is analogous to usual segregation, except the initial state has an off-critical composition. We know that the LS growth law applies for the diffusive phase separation, regardless of the mixture composition.[27–14] Therefore, the growth of the second length scale is characterized by the LS growth law with the "zero time" located at the time of the second quench t_2, i.e., $L_2(t) \sim (t - t_2)^{1/3}$. This growing length scale coexists with the larger length scale L_1, which is approximately static. If the second quench lasts sufficiently long, L_2 becomes comparable to L_1; subsequently, the system segregates in the usual manner.

D. Further heating and quenching

Now that the scenario is clear, we can generalize it to the case of multiple quenching and heating. For example,

we have performed a second heating simulation at $T = \infty$ by starting with the system at $t_3 = t_2 + 20\,000$ MCS (last snapshot in Fig. 5). We heat the system up to $t_3 + 25$ MCS, and the resultant evolution snapshots are shown in Fig. 7. In Fig. 8, we show the evolution of the structure factor during the second heating period. As expected, the structure starts melting at the smallest length scales, and this propagates to larger and larger length scales. The solid lines denote the expression in Eq. (11) with the appropriate functional form of $S(\vec{k}, t_3)$.

The third quench is performed at $t_4 = t_3 + 25$ MCS. The resultant evolution morphology in Fig. 9 has three length scales. The plot of $S(k, t)$ vs k in Fig. 10(a) shows that two of these are static and the third one increases with time. The time-dependence of these length scales is shown in Fig. 10(b). In general, n quenches give rise to a morphology with n length scales. However, we must be careful that the heating period is not so long that it washes out the structure existing at the end of the previous quench.

III. CAHN–HILLIARD–COOK MODEL WITH A TIME-DEPENDENT TEMPERATURE

In Sec. II, we have described a method to generate a multiscale structure for the Kawasaki–Ising model. Let us now approach this problem via the CHC model, which is the appropriate coarse-grained model for phase-separation dynamics. In this model, the system is described by an order parameter $\psi(\vec{r}, t) = \rho_A(\vec{r}, t) - \rho_B(\vec{r}, t)$, where ρ_A and ρ_B denote the local densities of species A and B. We use the dimensionless version of the CHC equation, which is obtained by a suitable rescaling of space, time, and order parameters,[28]

$$\frac{\partial}{\partial t}\psi(\vec{r}, t) = \vec{\nabla} \cdot \{\vec{\nabla}[\pm\psi + \psi^3 - \nabla^2\psi] + \vec{\theta}(\vec{r}, t)\}, \qquad (20)$$
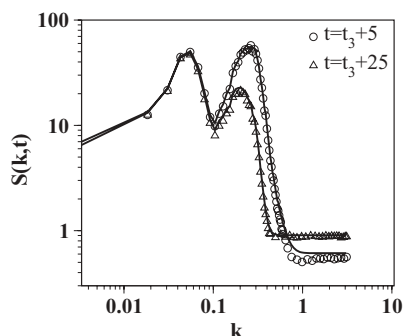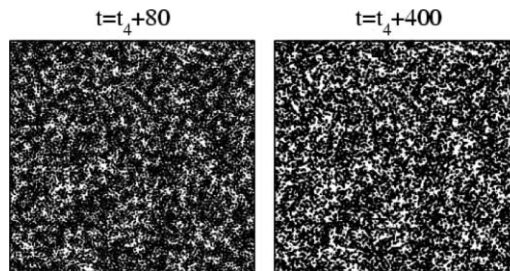

FIG. 8. Structure factors at two different times during the second heating period. The solid lines denote the expression in Eq. (11) with $S(k, t_1)$ replaced by $S(k, t_3)$ and $\sigma^2 = 2(t - t_3)$.
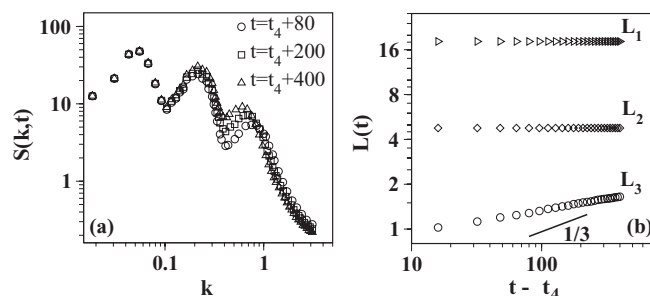

FIG. 10. (a) Structure factors at three times during the third quench period. (b) Time-dependence of domain length scales during the third quench period.

where

$$\langle \vec{\theta}(\vec{r}, t) \rangle = 0,$$
$$\langle \vec{\theta}_i(\vec{r}', t') \vec{\theta}_j(\vec{r}'', t'') \rangle = 2\epsilon \delta_{ij} \delta(\vec{r}' - \vec{r}'') \delta(t' - t''). \quad (21)$$

In Eq. (20), the $+$ sign corresponds to $T > T_c$ and the $-$ sign corresponds to $T < T_c$. For $T > T_c$, which corresponds to the heating period, the nonlinear term is not relevant.

We implemented a Euler-discretized version of Eq. (20) with an isotropic Laplacian on a square lattice of size $L \times L$ ($L = 512$). Periodic boundary conditions were imposed in both directions. The discretization mesh sizes in space and time were $\Delta x = 1.0$ and $\Delta t = 0.02$, respectively. The initial condition consisted of small fluctuations about $\psi_0 = 0$, i.e., a critical quench. Finally, the thermal noise of strength ϵ is mimicked by uniformly distributed random numbers between $[-A, A]$. (We obtain similar results if a Gaussian-distributed noise is used.) The appropriate noise amplitude in our Langevin simulation is

$$A = \sqrt{\frac{3\epsilon}{(\Delta x)^d \Delta t}}. \quad (22)$$

The results reported here correspond to $\epsilon = 0.000\,42$, i.e., $A = 0.25$ for $\Delta x = 1.0$ and $\Delta t = 0.02$. All statistical quantities are obtained as averages over ten independent runs on systems of size 512^2.

In Fig. 11, we show evolution snapshots for the CHC system subjected to alternating cycles of cooling and heating, i.e., switching between the $-$ and $+$ signs in Eq. (20). The system is evolved (a) at $T < T_c$ up to $t_1 = 20\,000$; (b) at $T > T_c$ up to $t_2 = t_1 + 500$; (c) at $T < T_c$ up to $t_3 = t_2 + 800$; and (d) at $T > T_c$ up to $t_4 = t_3 + 40$. The emergence of a two-scale structure is evident in the snapshot at $t_3 = t_2 + 800$, corresponding to the end of the second quench. As in the Kawasaki–Ising model, the cooling–heating cycles produce multiple length scales (see snapshots in Fig. 12 for the evolution after the third quench). The corresponding correlation functions and structure factors no longer show dynamical scaling. In Fig. 13, we show the structure factors at different stages of the evolution in Fig. 11. We show two datasets in the cooling periods $[t = 20\,000$ and $t = t_2 + 800$ in Fig. 13(a)] and two datasets in the heating periods $[t = t_1 + 100$ and $t = t_3 + 10$ in Fig. 13(b)]. As expected, $S(k, t)$ vs k in the cooling periods shows a Porod tail. The dataset for $t = t_2 + 800$ corresponds to the second quench and shows a two-peak structure [cf., Fig. 6(a)].

The datasets for $S(k, t)$ vs k in the heating periods show a characteristic flat behavior at large values of k. Their functional form can be obtained from the CHC equation for $T > T_c$,

$$\frac{\partial}{\partial t} \psi(\vec{r}, t) \simeq \vec{\nabla} \cdot [\vec{\nabla} \psi + \vec{\theta}(\vec{r}, t)]. \quad (23)$$

Equation (23) is obtained by neglecting the cubic and the fourth-derivative terms in Eq. (20). These terms are not relevant in the dynamics for $T > T_c$. Consider the case when the system is heated at $t = t_1$. We can solve Eq. (23) in
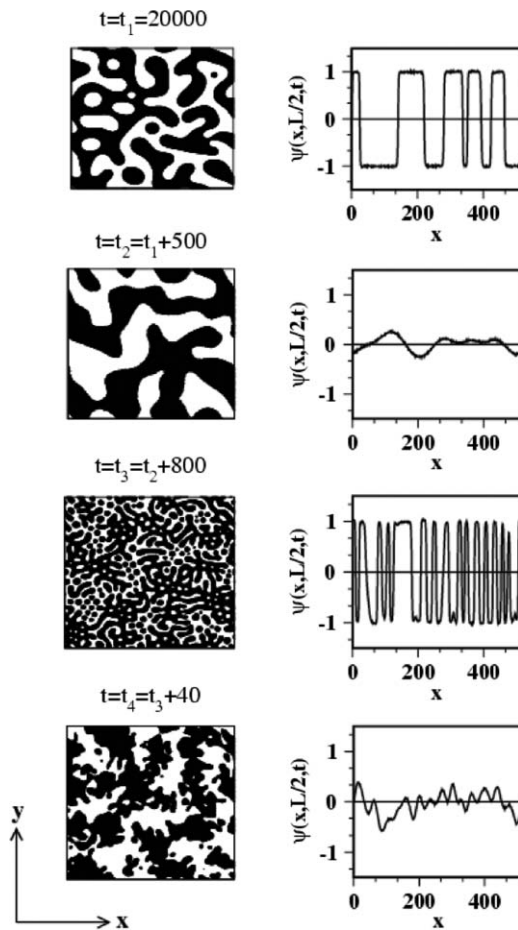

FIG. 11. Evolution snapshots for the CHC system subjected to alternate cycles of cooling and heating. The switching times are as follows: $t_1 = 20\,000$ (end of first quench), $t_2 = t_1 + 500$ (end of first heating), $t_3 = t_2 + 800$ (end of second quench), and $t_4 = t_3 + 40$ (end of second heating). The simulation details are provided in the text. Regions with $\psi > 0$ (A-rich) and $\psi < 0$ (B-rich) are marked in black and white, respectively. To the right of each snapshot, we show the variation of the order parameter along a cross-section at $y = L/2$, where L is the lateral system size.
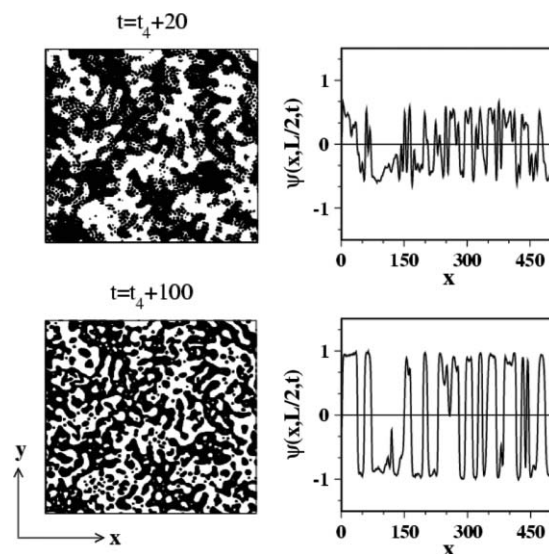

FIG. 12. Evolution snapshots for the CHC system after the third quench at $t_4 = 21\,340$.
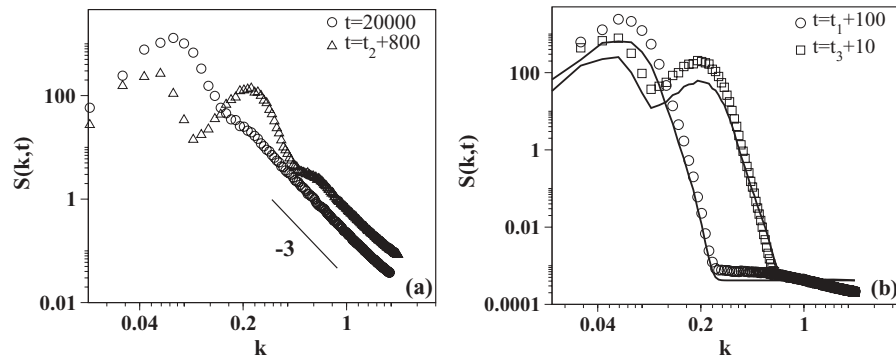
FIG. 13. Structure-factor data for the CHC evolution shown in Fig. 11. (a) Datasets during the quench periods (at $t = 20\,000$ and $t = t_2 + 800$). (b) Datasets during the heating periods (at $t = t_1 + 100$ and $t = t_3 + 10$). The solid lines denote the expression in Eq. (26) with the appropriate replacement for $S(\vec{k}, t_1)$.

momentum space as follows:

$$\psi(\vec{k}, t) = \psi(\vec{k}, t_1)e^{-k^2(t-t_1)} - i \int_0^{t-t_1} dt' e^{-k^2(t-t_1-t')}$$
$$\times [\vec{k} \cdot \vec{\theta}(\vec{k}, t')]. \tag{24}$$

This yields the structure factor as

$$S(\vec{k}, t) = \langle \psi(\vec{k}, t)\psi(-\vec{k}, t) \rangle$$
$$= S(\vec{k}, t_1)e^{-2k^2(t-t_1)} + e^{-2k^2(t-t_1)}$$
$$\times \int_0^{t-t_1} dt' \int_0^{t-t_1} dt'' e^{k^2(t'+t'')} \langle [\vec{k} \cdot \vec{\theta}(\vec{k}, t')]$$
$$\times [\vec{k} \cdot \vec{\theta}(-\vec{k}, t'')] \rangle. \tag{25}$$

Thus, $S(\vec{k}, t)$ is obtained in terms of $S(\vec{k}, t_1)$ as

$$S(\vec{k}, t) = S(\vec{k}, t_1)e^{-2k^2(t-t_1)} + \epsilon[1 - e^{-2k^2(t-t_1)}]. \tag{26}$$

The solid lines in Fig. 13(b) denote the functional form in Eq. (26) and are in reasonable agreement with the numerical data.

IV. SUMMARY AND DISCUSSION

Let us conclude this paper with a summary and discussion of the results presented here. We consider the effect of a time-dependent variation of temperature on the morphology of a phase-separating binary (AB) mixture. We find that alternate cycles of cooling and heating give rise to a multiple-length-scale morphology. During a quench period, the resultant pattern contains imprints of (static) length scales from previous quenches as well as a growing length scale from the most recent quench. On the other hand, during a heating period, there is a melting of the domain structure as the A, B particles perform random walks. We can use this picture to analytically obtain the structure factor $S(\vec{k}, t)$ during a heating period $[t_i, t_{i+1}]$ as a function of $S(\vec{k}, t_i)$.

To confirm the above scenario, we have presented results from (a) MC simulations of the Kawasaki–Ising model and (b) Langevin simulations of the CHC model. The numerical results are in excellent agreement with our analytical results. The fabrication of multiscale morphologies offers intriguing possibilities for technological applications, e.g., in food processing, paints, biomaterials. It also suggests the possibility that we can formulate temperature-variation protocols for the

manufacture of materials with predesignated morphologies. Our work in this paper is a modest first step in this direction.

In future, we intend to combine the work presented here with an earlier work on the phase separation of mixtures of immiscible polymers.[29] This will allow us to study the interplay of temperature variations and polydispersity.

[1] A. J. Bray, Adv. Phys. **43**, 357 (1994).
[2] *Kinetics of Phase Transitions*, edited by S. Puri and V. K. Wadhawan (CRC Press, Boca Raton, FL, 2009).
[3] S. K. Das, S. Puri, J. Horbach, and K. Binder, Phys. Rev. E **72**, 061603 (2005); Phys. Rev. Lett. **96**, 016107 (2006); K. Binder, S. Puri, S. K. Das, and J. Horbach, J. Stat. Phys. **138**, 51 (2010).
[4] S. J. Mitchell and D. P. Landau, Phys. Rev. Lett. **97**, 025701 (2006).
[5] M. J. A. Hore and M. Laradji, J. Chem. Phys. **132**, 024908 (2010).
[6] N. Blondiaux, S. Morgenthaler, R. Pugin, N. D. Spencer, and M. Liley, Appl. Surf. Sci. **254**, 6820 (2008).
[7] J. Liu, X. Wu, W. N. Lennard, and D. Landheer, Phys. Rev. B **80**, R041403 (2009).
[8] K. Kawasaki, Phys. Rev. **145**, 224 (1966).
[9] K. Kawasaki, in *Phase Transitions and Critical Phenomena*, edited by C. Domb and M. S. Green, (Academic, London, 1972), Vol. 2, p. 443.
[10] J. W. Cahn and J. E. Hilliard, J. Chem. Phys. **28**, 258 (1958); *ibid* **31**, 688 (1959).
[11] H. E. Cook, Acta Metall. **18**, 297 (1970).
[12] P. C. Hohenberg and B. I. Halperin, Rev. Mod. Phys. **49**, 435 (1977).
[13] I. M. Lifshitz and V. V. Slyozov, J. Phys. Chem. Solids **19**, 35 (1961).
[14] D. A. Huse, Phys. Rev. B **34**, 7845 (1986).
[15] C. Yeung, Phys. Rev. Lett. **61**, 1135 (1988).
[16] H. Furukawa, Phys. Rev. B **40**, 2341 (1989).
[17] G. Porod, in *Small-Angle X-Ray Scattering*, edited by O. Glatter and O. Kratky (Academic, New York, 1982), p. 42.
[18] A. O. Onuki, Phys. Rev. Lett. **48**, 753 (1982).
[19] D. Vollmer, J. Vollmer, and R. Strey, Europhys. Lett. **39**, 245 (1997); G. K. Auernhammer, D. Vollmer, and J. Vollmer, J. Chem. Phys. **123**, 134511 (2005); J. Vollmer, *ibid.* **129**, 164502 (2008).
[20] A. Turchanin and W. Freyland, Chem. Phys. Lett. **387**, 106 (2004); A. Turchanin, R. Tsekov, and W. Freyland, J. Chem. Phys. **120**, 11171 (2004).
[21] K. Binder and D. W. Heermann, *Monte Carlo Simulations in Statistical Physics: An Introduction* (Springer-Verlag, Berlin, 1988).
[22] M. E. J. Newman and G. T. Barkema, *Monte Carlo Methods in Statistical Physics* (Oxford University Press, Oxford, 1999).
[23] H. O. Carmesin, D. W. Heermann, and K. Binder, Z. Phys. B **65**, 89 (1986).
[24] Y. Oono and S. Puri, Phys. Rev. Lett. **58**, 836 (1987); Phys. Rev. A **38**, 434 (1988); S. Puri and Y. Oono, *ibid.* **38**, 1542 (1988).
[25] T. M. Rogers, K. R. Elder, and R. C. Desai, Phys. Rev. B **37**, 9638 (1988).
[26] I. S. Gradshteyn and I. M. Ryzhik, *Table of Integrals, Series and Products* (Academic Press, Burlington, 2007).
[27] S. Puri, Phys. Lett. A **134**, 205 (1988).
[28] S. Puri, in Ref. 2, pp 1.
[29] J. K. Wolterink, G. T. Barkema, and S. Puri, Phys. Rev. E **74**, 011804 (2006).